Relative current effect on short wave growth

Pedro Veras Guimarães, Fabrice Ardhuin, Yves Perignon, Alvise Benetazzo, Marie-Noëlle Bouin, Valerie Garnier, Jean-Luc Redelsperger, Mickael Accensi, Jim Thomson

Ocean Dynamics
August 2022, Volume 72 Issue 8 Pages 621-639
https://doi.org/10.1007/s10236-022-01520-0
https://archimer.ifremer.fr/doc/00787/89925/

Relative current effect on short wave growth

Veras Guimarães Pedro [2, 3, 6, *], Ardhuin Fabrice [6], Perignon Yves [2], Benetazzo Alvise [4], Bouin Marie-Noëlle [6], Garnier Valerie [1], Redelsperger Jean-Luc [6], Accensi Mickael [1], Thomson Jim [5]

[1] Laboratoire d'Océanographie Physique et Spatiale, Univ. Brest, CNRS, Ifremer, IRD, 1625 Route de Sainte-Anne, Plouzané, 29280, Finestèr, France
[2] LHEEA lab UMR6598, École Centrale de Nantes, 1 Rue de la Noë, Nantes, 44300, Pays de la Loire, France
[3] Graduate Program in Ocean Engineering (PPGEO), Federal University of Rio Grande - FURG, Av. Itália, s/n - km 8, Rio Grande, 96203-900, RS, Brazil
[4] Istituto di Scienze Marine (ISMAR), Consiglio Nazionale delle Ricerche (CNR), Arsenale Castello, 2737/F, Venice, 30122, VE, Italy
[5] Applied Physics Lab, University of Washington, Henderson Hall (HND), 1013 NE 40th St, Seattle, 98105, WA, USA
[6] Laboratoire d'Océanographie Physique et Spatiale, Univ. Brest, CNRS, Ifremer, IRD, 1625 Route de Sainte-Anne, Plouzané, 29280, Finestèr, France

* Corresponding author : Pedro Veras Guimarães, email address : pedro.guimaraes@furg.br

Abstract :

Short waves growth is characterized by nonlinear and dynamic processes that couple ocean and atmosphere. Ocean surface currents can have a strong impact on short wave steepness and breaking, modifying the surface roughness, and consequently their growth. However, this interplay is poorly understood and observations are scarce. This work uses in situ measurements of near-surface winds, surface current, and waves under strong tidal current conditions to investigate the relative wind speed effect on the local short waves growth. Those observations were extensive compared with numerical modeling using WAVEWACHIII, where the simulations repeatedly fail to reproduce the observed wind sea energy under strong current conditions. Our field observations and coupled ocean-atmosphere numerical simulations suggest that surface currents can strongly modulate surface winds. That is a local process, better observed closer to the boundary layer than at 10 m height. Yet, it can cause a significant impact on the local wind shear estimation and consequently on the local waves' growth source term. The results presented here show that the relative wind effect is not well solved inside spectral waves models, causing a significant bias around the peak of wind sea energy.

Keywords : Air-sea interaction, Wind waves, Waves growth, Strong current

1 Introduction

Short waves growth is characterized by nonlinear and dynamic processes that couple ocean and atmosphere. Winds blowing over the ocean transfers momentum and energy from the atmosphere to the ocean. A small portion of the wind momentum is directly transformed into current momentum, and the rest is responsible for wave generation and growth. The feedback of the airflow on the waves is the main mechanism that explains wave growth (Miles, 1957).

From the preliminary ripple to the fully grown waves, the air-sea interface is characterized by nonlinear and dynamic processes that couple ocean and atmosphere. However, this coupling is usually partially neglected in forecast models, in which winds, currents, and waves are usually computed separated. This is particularly important on the ocean mixed layer that has a strong impact of momentum and turbulent kinetic energy exchange in the between ocean and atmosphere, with a clear impact in the atmospheric boundary layer (Sullivan and Mcwilliams, 2010). The works of Black et al (2007) and Edson et al (2007) attempt to connect coupled marine-atmospheric dynamic boundary layers over high and low wind speeds. Edson et al (2007) results suggest that the mesoscale ocean process can modulate the air-sea momentum and heat exchange, which may have an important impact on the mesoscale atmosphere forecast.

Waves are also sensitive to the upper ocean circulation conditions. Ocean currents, induce wave refraction and dissipation (Kudryavtsev et al, 1995; Ardhuin et al, 2012; Rapizo et al, 2016). Current can dramatically increase the local density of wave energy, contributing to the appearance of extreme waves (Gutshabash and Lavrenov, 1986; White and Fornberg, 1998). This enhancement of wave heights is somewhat limited by wave breaking (Phillips, 1984; Ardhuin et al, 2012). Indeed, the changes in wave steepness can lead to a preferential breaking of waves in regions of strong current. From that observation, Phillips (1984) pointed out that in this situation the waves energy dissipation should be a nonlinear function of the wave steepness.

There is vast literature on the theoretical effects of currents on wind-wave propagation, leading to many numerical wave modeling developments over the past two decades. Although, there are unfortunately very few validations of realistic numerical modeling of waves in currents, especially under strong current conditions (e.g., Masson, 1996; van der Westhuysen et al, 2012; Ardhuin et al, 2012). From observations and numerical experiments, Ardhuin et al (2012) points out that in some macro-tidal environments the strong tidal current conditions can greatly influence the wave fields with induced variations up to 30% of the significant wave height.

In general, the sea state conditions are the results of a subtle coupled balance between the atmospheric and oceanic boundary layers, and any dynamical process in one or the other can have a significant impact on wave properties. Because of that, the accuracy of numerical wave models relies on the accuracy of its forcing input fields, and the parameterizations of the balance between its main source and sink terms that are the wind-wave generation, non-linear transfers, and dissipation (Komen et al, 1994; Janssen, 2008). A wide range of forcing conditions has indeed motivated the development of theoretical and numerical models of wave-current interactions (Leibovich, 1983; Thorpe, 2004).

In numerical wave models the wind speed imposed are usually defined at 10 m height (U_{10}), and the friction velocity ($u_\star$) is estimated from inside the model. The wind stress is obtained from the wind speed and a surface roughness length z_0 according to the Monin-Obukhov Similarity Theory (MOST), under these assumptions, the wind speed follow a logarithmic profile as a function of height (z).

$$\mathbf{U}(z) = \frac{\mathbf{u}_\star}{\kappa} \log\left(\frac{z}{z_1}\right) \tag{1}$$

where κ is the Von Kármán constant (~ 0.41) and z_1 is a fixed one meter elevation. Nowadays, most stochastic waves models use a relation based on Janssen (1991) to compute z_1, estimated from surface roughness length and friction velocity,

$$z_1 = \frac{z_0}{\sqrt{1 - \tau_\mathbf{w}/\tau_\mathbf{s}}} \tag{2}$$

where $z_0 = \alpha_0 u_\star^2/g$, $\tau_s = u_\star^2$ is the surface stress and τ_w is the wave-supported stress (see Janssen, 1991; Ardhuin et al, 2010, for more details). According Charnock (1955), the friction velocity and roughness length can be fairly well estimated by $z_0 = 0.015 u_\star^2/g$. So, from those equations it is possible to relate the wind stress to the wind speed,

$$\tau_\mathbf{s}/\rho_a = C_D \mathbf{U}_{10}^2, \tag{3}$$

where C_D is the surface drag coefficient and ρ_a is the air density (e.g. Edson et al, 2013). This equation gives a constant stress approximation, considering no wind turning between U_{10} to $u_\star$, also known as Bulk Formula. This Bulk Formula gives the friction velocity information, which is the most significant attribute of the wind input source term at stochastic waves models (see

The WAVEWATCH III® Development Group, 2016, for more implementation details).

In the presence of currents (on a moving surface), the absolute wind ($\mathbf{U}_{\text{abs}}$) must be correct by the relative wind ($\mathbf{U}_{\text{rel}}$) and the current velocity ($\mathbf{C}$). This is necessary to satisfy the boundary condition at $z = 0$, as so $\mathbf{U}_{abs}(z = 0) = \mathbf{C}$ (Hersbach and Bidlot, 2008). So the generation of waves by the wind can be formulated in the frame of reference in which the surface current is zero, for that is convenient to define a relative wind,

$$\mathbf{U}_{\text{rel}}(z) = \mathbf{U}_{\text{abs}}(z) - \mathbf{C}. \tag{4}$$

Than this relative wind comes into the wind-wave growth parameterization via Bulk Formula (Eq.3) by replacing $\mathbf{U}_{10}$ for $\mathbf{U}_{10,\text{rel}}$. For numerical implementation, Hersbach and Bidlot (2008) considered a simple reduction coefficient r_{wnd}, applied to the wind vector at the lowest model level ($z = 10$). Which gives,

$$\mathbf{U}_{10,\text{rel}} = r_{\text{wnd}}(\mathbf{U}_{10,\text{abs}} - \mathbf{C}) \tag{5}$$

According to Hersbach and Bidlot (2008), at the lower wind model level, near 10 m, $r_{\text{wnd}} \sim 1$ and by comparing with many buoys measuring wind at a height of 4 or 5 m, $r_{\text{wnd}} < 1$. However, the same authors found that the effect on surface stress is smaller that what would have been intuitively obtained by subtracting the ocean current from the surface wind of a system ($r_{\text{wnd}} < 1$).

Besides Hersbach and Bidlot (2008), the number of simultaneous observations of current, wind, and waves is still very scarce. Because of that, in this paper, we aim to explore the processes which interact with the free surface kinematics (waves, currents, and atmospheric interactions), their impacts on the shape of the waves spectrum, and their numerical implications. For that, the next section 2 presents an experiment, that was particularly designed to measure air-sea interactions under strong tidal current conditions and the numerical simulations used to compare with those experimental results. Section Section 3 compare the performance of the numerical stochastic wave model (using different parameterizations for wind input and dissipation) with in situ experiments acquired under natural tidal current conditions in the North West of France. Based on those results, a discussion about the unsatisfactory model results under strong current conditions is raised in section 4.

2 Methods

A few dedicated experiments in the laboratory and field have provided data on wave-current interactions, in particular at inlets or river mouths with a focus on wave blocking by the current (e.g. Masson, 1996; Chawla and Kirby, 2002; van der Westhuysen et al, 2012; Ardhuin et al, 2012; Dodet et al, 2013; Zippel and Thomson, 2017; Rapizo et al, 2017). Also, several remote sensing observations have shown interesting features induced by currents on surface roughness (Kudryavtsev et al, 2005; Rascle et al, 2014, 2016, 2017), which is

related to the properties of short gravity waves. To combine observation of dominant waves (swell) and shorter waves (wind sea) and understand the complex interaction of wind, waves, and currents, a series of experiments designed to explore a wide range of the wave spectrum was designed and carried out. The results presented here were part of the "Broad-Band WAVES" (BBWAVES) experiments, performed in 2015 and 2016, to explore questions related to the interactions between swell and wind sea waves, in the presence of strong tidal current on the Northwest coast of France.

Some experimental results obtained during the BBWAVES campaigns and are used here to compare with WAVEWATCH III model results. The model is used to provide a context to point measurements and the data are also used to evaluate the model capabilities and performance in regions of strong current.

2.1 BBWAVES Experiment

The 2015 BBWAVES experiment was carried out from 22 to 29 October in the region 5.16°W–4.76°W and 48.26°N–48.53°N (see, Fig.1). According to Muller et al (2007), the mean depth in this area is 110 m, the interaction with the coastline and bathymetry causes strong currents along the North coast (1.55 m/s), around Sein and Ushant islands. The tidal wave in this area is semi-diurnal and propagates northwards at the extreme end of Brittany. It is a meso-tidal region with a typical spring tidal range of 6 m and currents exceeding 2 m/s around islands and headlands, in constricted areas during spring tides the surface currents can reach up to 4.11 m/s in certain fairways (Muller et al, 2007; Ardhuin et al, 2012). Ardhuin et al (2009) mentions that the currents in this region are strongly dominated by tides with a near-inertial component driven by winds that only accounts for about 2% of the current variance. This makes the currents in this area well predictable and favors the definition of specific sea conditions to deploy the equipment to investigate strong currents conditions.

A second BBWAVES campaign was conducted between 21st to 27th September 2016, under similar sea state conditions, aiming to validate and verify the observations on the previous one. During the campaigns were observed currents ranging from 1.26 to 3.61 m/s.

In order to measure the wave conditions along the current in this area we used a ship-mounted stereo video wave system (Fig.2.a), six drifter buoys (Fig.2.d) especially developed and tested to measure the waves under current conditions (see, Guimarães et al, 2018) and for BBWAVES 2016 were also added a two SWIFT buoys developed by Thomson (2012, Fig.2.b). In addition, at several locations, a small trimaran (OCARINA, Bourras et al, 2014, see Fig.2.c) designed for the estimation of air-sea fluxes at the atmospheric surface boundary layer, were used to collect data next to the wave sensors. Figure 2 shows the main equipments used during the experiments and the next sections are dedicated to briefly introducing those equipments and the main setup used.

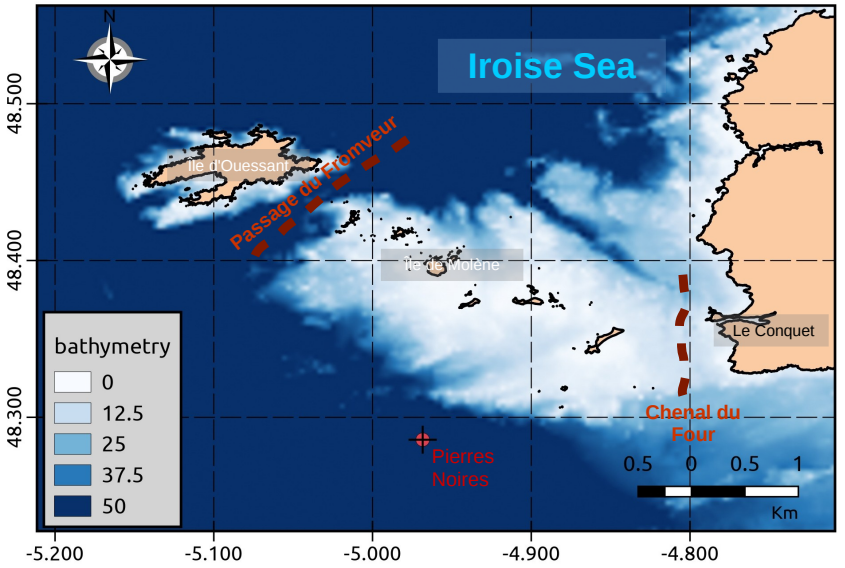

Fig. 1 Study field at Iroise Sea. The red dash lines mark the position of the main current features analyzed in this study and the red dot mark the moored Datawell buoy, Pierres Noires, used to validate the equipments used here.

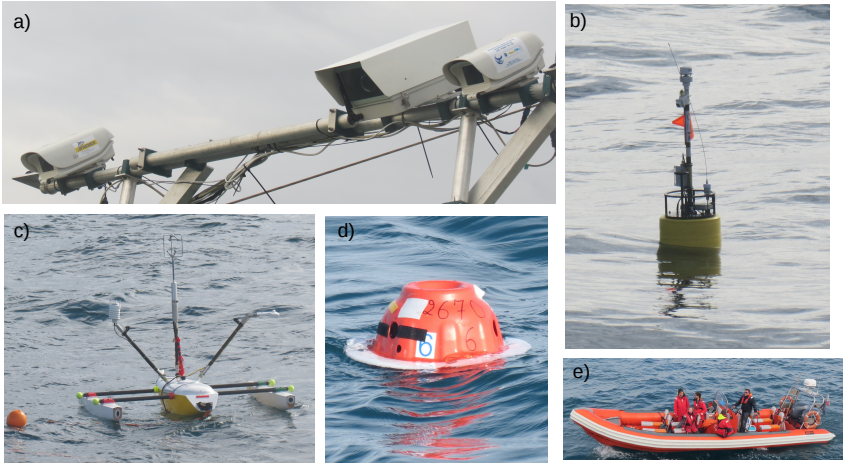

Fig. 2 Main equipment and sensor used during the BBWAVES 2016 experiments: a) Stereo video system, b) SWIFT buoy, c) OCARINA, d) SKIB buoy, e) Zodiac boat

2.1.1 SKIB buoys

For BBWAVES 2015 and 2016, it was used six 'Surface KInematic Buoys' (SKIB Guimarães et al, 2018) particularly optimized for the measurement of waves-current interactions, including relatively short wave components (relative frequency around 1 Hz). They combine a GNSS receiver with a

motion-sensor package. These buoys drift with the surface current and provide unique measurements of wave-current interactions. A comparison with existing Datawell Directional Waverider and SWIFT buoys, as well as stereo-video imagery are presented in Guimarães et al (2018).

2.1.2 SWIFT buoys

For the BBWAVES 2016 campaign, it was used two Surface Wave Instrument Float with Tracking (SWIFT) buoys developed by Thomson (2012, Fig.2.b). The SWIFT is a small spar buoy with a 0.3 m diameter and 2.15-m height, developed to measure and image wave breaking in a wave-following reference frame. This buoy is equipped with a Microstrain 3DM-GX3-35 motion sensor and GPS receiver, a Nortek Aquadopp HR 1 MHz Doppler velocity profiler, an autonomous meteorological station, a digital camera, a real-time tracked radio frequency transmitter, and an ultrasonic anemometer (AirMar PB200). The spectra for each 520-second burst are calculated as the ensemble average of the fast Fourier transform of 16 sub-windows with 50% overlap, which results in 32 degrees of freedom. Besides, the SWIFT horizontal velocity data from the phase-resolving GPS contain the wave orbital motions relative to the Earth reference frame.

2.1.3 Ship-mounted stereo-video system

The general principle of 3D surface reconstruction is presented by Benetazzo (2006); Leckler (2013); Benetazzo et al (2016); Guimarães (2018). In the Lagrangian reference associated with the moving ship, the center point of the field needs to be accounted for. For that, a compact Inertial Navigation System with integrated Dual-antenna GNSS[1] receiver Ellipse2-D is then used for this purpose. It includes a MEMS-based Inertial Measurement Unit (IMU) and runs an enhanced Extended Kalman Filter (EKF) which fuses inertial and GNSS data. It provides Roll, Pitch, Heading, Heave, and Navigation data (see Guimarães, 2018, for more details of the ship motion correction).

The 30 min stereo video results were gridded over 10 m $\times$ 10 m square surface with 0.1 m resolution, where x, y represent the longitude and latitude in UTM. The 3D spectrum $E(k_x, k_y, f)$ was obtained after applying a Hamming window in all three (x, y, t) dimensions to the elevation maps over time intervals of 85.33 seconds (1024 frames), with 50% overlapping. As a result, the energy over frequency and waves number are acquired in a Lagrangian reference frame, and the Doppler shift in σ must be corrected by the mean boat velocity ($\mathbf{U_b}$) over the 1024 time window. So the apparent frequency is corrected by $\sigma_c = \sigma - \mathbf{k} \cdot \mathbf{U_b}$. Consequently, the heave frequency spectrum $E(f)$ is obtained by integration of the 3D spectrum and it is expressed in terms of the absolute frequency ($\omega = \sigma_c + \mathbf{k} \cdot \mathbf{U} = 2\pi f_a$).

[1] Global Navigation Satellite System

2.1.4 OCARINA wind platform

The wind measurements near the surface were collected by the OCARINA (Ocean Coupled to Atmosphere, Research at the Interface with a Novel Autonomous platform Bourras et al, 2014). This is a 2 m long trimaran floating platform specifically designed for the estimation of air-sea fluxes in the lower atmospheric boundary layer to investigate wind-wave interactions. The system was deployed from the research vessel and let freely drifting over the current fields analyzed here.

The equipment installed in the OCARINA uses a Vaisala WXT-520 meteorological station to measure the air temperature and humidity, static pressure, rain, and wind, at 1 Hz. This meteorological instrument package was placed at a low elevation above the waterline (1 m). An inertial motion unit (IMU) was placed at the horizontal center of OCARINA and the level of the waterline. The inertial motion unit is an Xsens MTI-G device, which features three magnetometers, three accelerometers, three gyroscopes, a GPS, and a barometer.

2.1.5 Experimental conditions

For the BBWAVES 2015 and 2016 experiments, it was possible to measure wind and waves in areas of strong currents. Figure 3 summarize the main wind, current conditions, and buoys track. The drift of the buoys over the current structure, the color lines represent the 10 minutes path used to compute the spectrum, starting in red. The wind velocity and field of current intensity are presented in those figures representing the WW3 forcing conditions at the beginning of the SKIB acquisition. A spatial 10 min average between the six synchronized buoys was used to evaluate the space and time evolution of the wave field over the current structure.

The acquisitions presented here were carried mostly under moderate wind conditions, with speeds from 3 to 7 m/s. The current conditions pictured Figure 3 a to c vary from 1.26 to 2.22 m/s. For reference, the average dominant wave information's (Hs and Tp) across the experimental path is summarize on Figure 3. Nevertheless, to further verify the instrumental accuracy, the observed difference between the model output and the instruments were also obtained from the SWIFT buoys (SC5, Fig.3.e) and ship-mounted stereo video system (SC4, Fig.3.d) under similar conditions.

In selected case 1 (SC1, Fig.3.a) the SKIB were deployed in the Passage du Fromveur, with a light breeze from South, the relative wind and the current direction is about 40^o. SC2 (Fig.3.b) presents similar atmospheric conditions to SC1, however, at SC2 the drifting buoys were placed at the edge of Passage du Fromveur, with a decreasing current speed from 1.73 to 1.05 m/s. Because in SC1 and SC2 the wind component has some alignment with the meridional buoys velocity, in these two cases it was considered that the short wave field is more or less following the current flow.

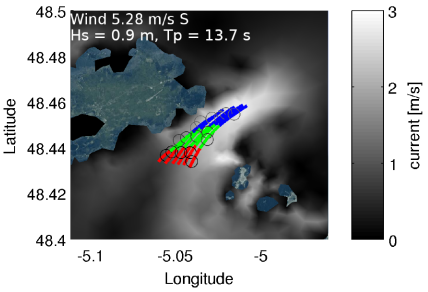

(a) SC1: SKIB 2015/10/23 08:30 to 09:00

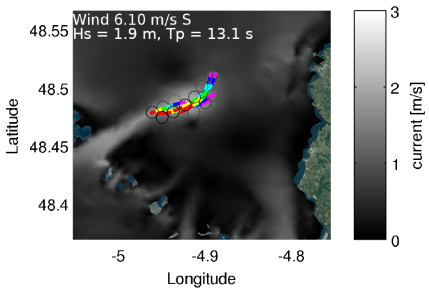

(b) SC2: SKIB 2015/10/23 10:30 to 11:30

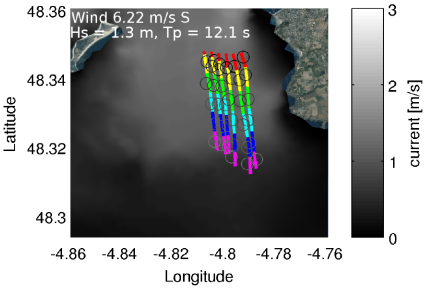

(c) SC3: SKIB 2015/10/23 13:40 to 14:40

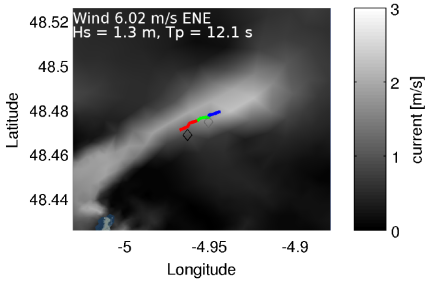

(d) SC4: Stereo video 2015/10/23 10:04 to 10:34

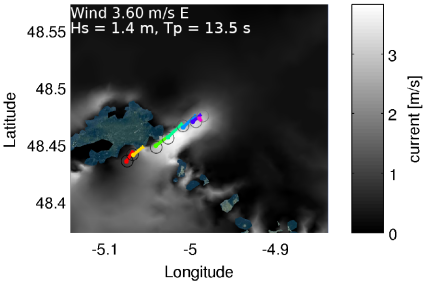

(e) SC5: SWIFT at 2016/09/21 15:08 to 16:32

Fig. 3 Experimental conditions during BBWAVES 2015 and 2016. The colormap shows the local current conditions during the experiment, the 10 minutes drifting buoys (or stereo video, d) segments of the path are synchronized and marked by different colors. The current direction is the same as drifting buoys path starting in red (for d, the boat was also following the current). The gray circles represent the selected WW3 grid point output positions. The local wind conditions at 10 m considered in the model are labeled in white in the figures. The current and wind information presented in the figure are the same used to force ST4 numerical test describe in the next section (Sec.2.2). The dominant significant wave height (Hs) and peak period (Tp) are presented below the wind data.

On the other hand, SC3 (Fig.3.c) is characterized by a short wave and current propagating in an opposing direction. At SC3 the buoys were deployed in Chenal du Four, over an increasing current varying from 1.26 to 1.49 m/s. The wind waves were created by a 6.22 m/s South wind and propagating against this tidal current field.

SC4 and SC5 (Fig.3.d and Fig.3.e) present a relative similar current conditions to the ones analyzed in SC1 and SC2, respectively. However, in these cases, the wind (U_{10}) relative to the current (from buoys propagation direction) are supposed to be almost in opposing directions. SC5 also presents the strongest current condition analyzed here, where the drifting speeds vary from 1.4 to 3.6 m/s. These SC4 and SC5 cases are of particular interest because we also had measurements with the OCARINA and SWIFT. The local wind, wave, and current conditions appear in Figure 3 (d and e) were collected from the OCARINA and SWIFT instruments.

2.2 Numerical experiment

Intending to evaluate how the spectral wave model WAVEWATCH III (WW3, version 4.18 from Tolman et al, 2014) performs under realistic current conditions, we did several numerical tests. The simulations for the tests use the advection schemes over unstructured grids, implemented by Roland (2008), and most of the source functions for wave dissipation and generation follow the ones used in reference test case "TEST471" from Ardhuin et al (2010). The nonlinear waves interactions were modeled using the Discrete Interaction Approximation (DIA, Hasselmann et al, 1985).

The simulations were done using a high-resolution triangular mesh over the Iroise Sea, with a higher definition at high gradients of bathymetry areas and around the islands, where it is expected to observe stronger current conditions (Fig.4). The spatial resolution varies from $\sim$ 100 m close to the islands to $\sim$ 5 km close to the oceanic boundary. The spectral resolution considers 32 frequencies and 24 directions. The period studied corresponds to the same time as BBWAVES experiments.

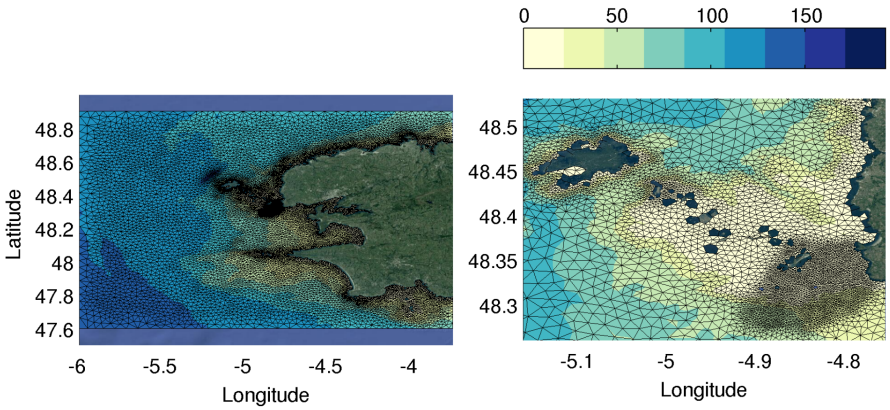

Fig. 4 Bathymetry and mesh of the Iroise Sea area. Plot (a) present the whole area used for wave computation, while (b) is a zoom of the same mesh, refined in the areas of strong current observations.

The boundary conditions, in the form of directional wave spectra, are provided by hindcasts over the global ocean (Rascle and Ardhuin, 2013) and a nested mesh over the Bay of Biscay and English Channel (NORGASUG), that has been carefully validated against buoy and satellite altimeter data (Roland and Ardhuin, 2014). These are available at ftp.ifremer.fr/ifremer/ww3/HINDCAST/NORGASUG/. These model configurations are forced by European Center for Medium-Range Weather Forecasts (ECMWF) operational winds and tidal currents from a barotropic model (Ardhuin et al, 2012). The models use the parameterization by Ardhuin et al (2010) as updated by Rascle and Ardhuin (2013) and the TEST471 settings for the input and dissipation (The WAVEWATCH III ® Development Group, 2016). These offshore boundary conditions are generally accurate in terms of wave heights and mean periods, with normalized root mean square errors (NRMSEs) less than 10% for Hs offshore.

Our model grid is forced by the same current and water level model as the parent WAVEWATCH III grid, using a 250 m resolution hindcast implementation of MARS2D (Model for Application at Regional Scale, Lazure and Dumas, 2008). That implementation is described by Pineau-Guillou (2013). A comparison between the current forcing field and the observed surface current by SKIB and SWIFT drifting buoys are presented at Figure 5.

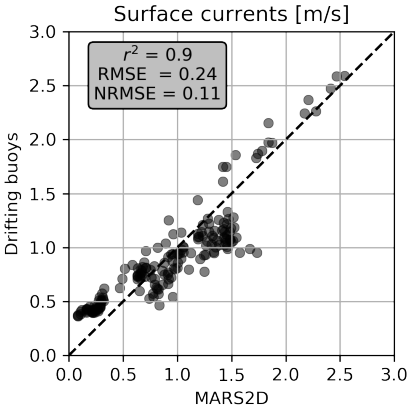

Fig. 5 Comparison between the local current speed from MARS2D (Pineau-Guillou, 2013) and the average drifting speed from SKIB and SWIFT buoys. In the inside box it is presented the Pearson correlation coefficient (r^2), Root Mean Square Error (RMSE) and the Normalized Root Mean Square Error (NRMSE) computed from scipy statistics package (Virtanen et al, 2020).

For the wind forcing, it was used the ECMWF operational analyses and forecasts, giving a time resolution of 3 hours on a $0.125° \times 0.125°$ of the spatial grid. An alternative wind source was tested over the same configuration using the Meteo-France small scale numerical prediction model (AROME, Ducrocq et al, 2005) with hourly output over a finer 2.5km grid.

Another aspect tested was the relative wind "RWND" correction. In WW3, this correction on the wind speed that forces the wave growth is taken as a correction factor, with $\mathbf{U}_{\text{model}} = \mathbf{U}_{10} - r_{\text{wnd}}\mathbf{C}$. This effect was found to be potentially important for tidal currents at coastal scales (Ardhuin et al, 2012).

2.2.1 Coupled winds and currents forcing

It was also tested a wind forcing coming from a coupled numerical simulation using the Meso-NH (Lafore et al, 1998) and MARS3D (Model for Application at Regional Scale, Lazure and Dumas, 2008) models. The Meso-NH is a non-hydrostatic meso-scale atmospheric model that deals with different scales, ranging from large (synoptic) to small (large eddy) scales and allows a multi-scale approach through a grid-nesting technique. The MARS3D is a three dimensional hydrodynamical model developed to provide realistic descriptions of coastal phenomena. These two models were couple by a standard coupling interface in the SURFEX surface model (Masson et al, 2013) following the same implementation done by Voldoire et al (2017). In this strategy, the sea surface moment flux and heat transfer between ocean and atmosphere are recomputed inside of each modeling timestep, constantly modifying the boundary conditions and consequently the near oceanic and atmospheric circulation.

Two Meso-NH simulations were done for BBWAVES 2015. One simulation was coupled with sea surface temperature and current (STC) from a 500x500 m MARS3D (Lazure and Dumas, 2008) and another simulation was forced with the same parameters but without current (NC). The atmospheric boundary condition for Meso-NH comes from the Meteo-France operational Arome winds every 3h. The Meso-NH was run on a 1.250×1.250 km horizontal grid resolution, 55 vertical levels, from 22/10/2015 00:00:00 to 24/10/2015 00:00:00 UTC corresponding to BBWAVES 2015 experiment.

2.2.2 Ad hoc correction of wind bias

For records where near-surface wind measurements were available, it was tested an ad hoc wind correction, in those cases the ECMWF forcing was multiplied by a constant factor R: $\mathbf{U}_{10}^{\text{ECMWF}} \times R$. This correction factor is calculated based on the near-surface wind measurements from OCARINA and SWIFT, extrapolated to 10 m height. For the cases that we do not have the local wind information, so it was corrected by an a priori constant coefficient. These numerical tests follow ST4 parameterization with the only modification in the forcing fields (according to test WNDxR in Tab.1).

2.2.3 Summary of numerical tests

We have thus investigated the accuracy of the wind forcing and tested a wide range of numerical model options. Table 1 shows the most representative parameters tested.

To compare the differences between the observed and modeled at each frequency, for different time and positions, we use the mean space and time

Table 1 Numerical tests, source term parameterizations, and adjustments of parameters and wind forcing. The conditions in bold are the value, forcing, or source function modified. ST4 is our controlled simulation with default values defined as TEST471 in The WAVEWATCH III ® Development Group (2016). BJA is an abbreviation for the parameterization by Bidlot, Janssen, and Abdallah (2005), which is activated by the ST3 switch in WW3, and mostly differs from ST4 by a global definition of wave steepness used for the dissipation parameterization. M2D is an abbreviation for the MARS2D hydrodynamic forcing field. COUP is the wind and currents forcing from the coupled simulation (Sec.2.2.1) and WNDxR is an ad hoc wind correction (Sec.2.2.2).

	Source package				Breaking		Forcing		
Test	S_{in}	S_{ds}	S_{nl}	r_{wnd}	$C_{\mathrm{ds}}^{\mathrm{sat}}$	B_r	WND	WL	CUR
ST4	T471	T471	DIA	1.0	-2.2×10^{-5}	0.0009	ECMWF	M2D	M2D
AROME	T471	T471	DIA	1.0	-2.2×10^{-5}	0.0009	**AROME**	M2D	M2D
RWND=0	T471	T471	DIA	**0.0**	-2.2×10^{-5}	0.0009	ECMWF	M2D	M2D
COUP	T471	T471	DIA	1.0	-2.2×10^{-5}	0.0009	**COUP**	**COUP**	**COUP**
WNDxR	T471	T471	DIA	1.0	-2.2×10^{-5}	0.0009	$U_{10}^{\mathrm{ECMWF}} \times \mathbf{R}$	M2D	M2D
No current	T471	T471	DIA	1.0	-2.2×10^{-5}	0.0009	ECMWF	M2D	**0.0**
ST3	**BJA**	**BJA**	DIA	1.0	–	–	ECMWF	M2D	M2D
SDSC2=0	T471	T471	DIA	1.0	**0.0**	0.0009	ECMWF	M2D	M2D

spectral density and standard deviation of the variance spectral density for different model configurations and acquisitions.

3 Results

Here we compare the BBWAVES experimental conditions presented at Figure 3 with the WW3 numerical tests (Tab.1). The model and observational results are compared in terms of the spectral density of the surface elevation variance, focusing on the wind sea peak frequencies (between 0.08 to 0.70 Hz), where it is expected to observe the highest impact induced by the currents because of the phase speed is closer to the current velocity. Lower frequencies (swell) will not be presented or discussed here as they are less susceptible to local wind speed and current transformations. The WW3 output of this variance $E(f)$ was used over the mesh grid points over the path of the buoys and at each 10 minutes intervals. We note that both the model and buoy data are relative frequencies, in the frame of reference moving with the current.

A spatial 10-min average between the six synchronized buoys was used to evaluate the space and time evolution of the wave field over the current structure. Figure 6 shows the experimental and numerical results for BBWAVES experiments in terms of the spectral density of the variance of sea surface elevation and its evolution in time, from the model in dashed lines and the buoys in solid colored lines. The solid lines represent the 10 minutes path used to compute the spectrum, starting in red. The model results presented here are labeled as $ST4$ (Tab.1) and uses the wind input and dissipation parameterizations from Ardhuin et al (2010), with adjusted parameters "TEST471" described by The WAVEWATCH III ® Development Group (2016).

The result presented here are limited to short wave frequencies (from 0.08 to 0.6 Hz), where it is observed bigger difference between the modeled and the observed. Considering these results (and others not shown here) it was

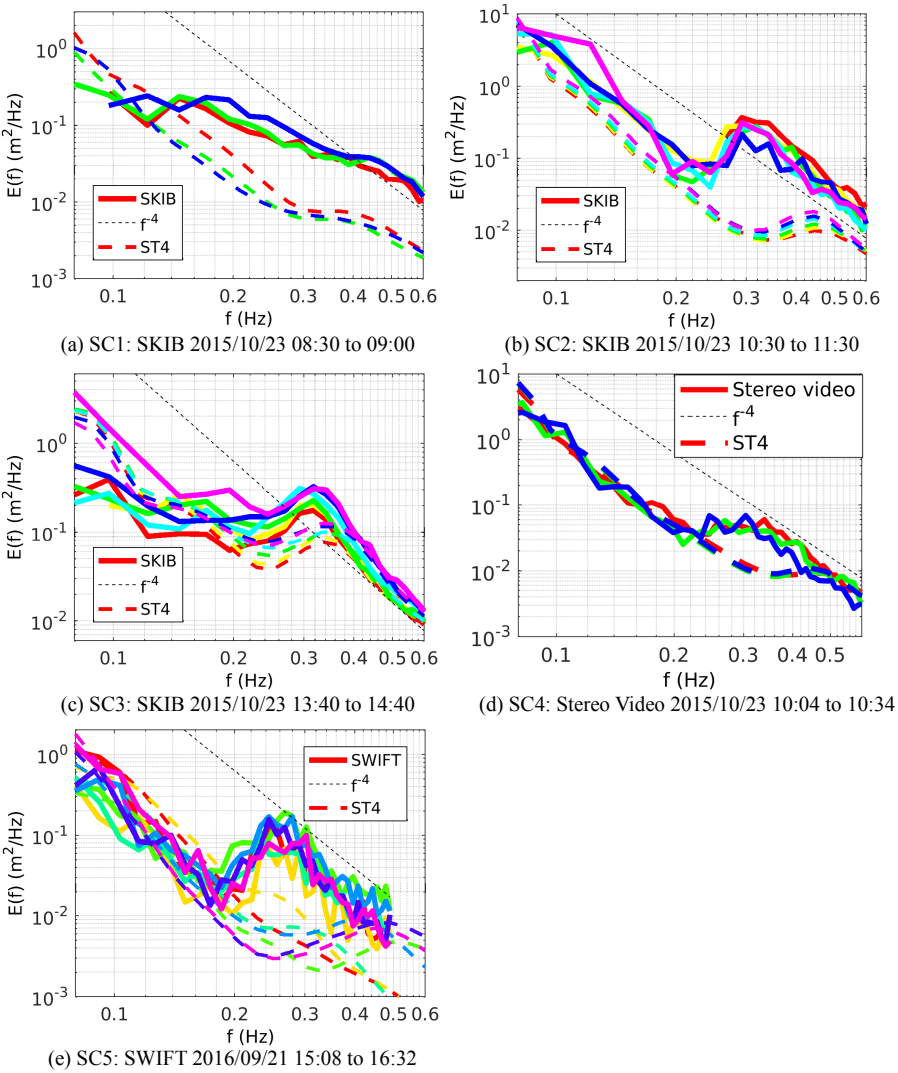

Fig. 6 Model and observational spectral density of the 10 minutes average spectral density of the variance and its evolution in time. The results for SKIBs are presented as a spatial average between the six synchronized buoys. The measurement results are displayed in solid color lines and the same quantity from the model is presented in dashed lines. The color patterns follow the conditions presented in Figure 3.

observed that the model tends to strongly underestimate the wind sea spectral components over ∼1.2 m/s currents (see Figs. 3 and 6). Those very general observations have led us to investigate these cases of stronger current conditions, where the WW3 model fails.

Note that the instruments used in this experiment were carefully tested and validated by Guimarães et al (2018), those buoys presented the best performance in the frequency range target on this work (from 0.07 Hz and up to 1 Hz). Nevertheless, to further verify the instrumental accuracy, the observed difference between the model output and the instruments were also obtained from the SWIFT buoys and ship-mounted stereo video system under similar conditions.

For the records SC5 and SC4 the wind forcing data were compared with the SWIFT and OCARINA data collected at 1 m (U_1) height and extrapolated to 10 m (U_{10}) height using a constant $z_0 = 0.0002$ approximation. It was observed very large differences in the wind directions between model forcing and the measurements, as indicated in Table 2.

Table 2 SC4 and SC5 wind and current conditions provided by the ECMWF operational model, compared with wind measurements from OCARINA and SWIFT, respectively. The wind direction is referenced by where the wind comes from. The MARS2D and the observed current C and C_{dir} are also given for reference. The current direction is given by the direction where the current is going.

		SC4			SC5					
	Δt	34	12	12	12	12	12	12	12	min
Model	C	1.4	1.0	1.1	2.9	3.3	1.8	2.5	2.0	m/s
	C_{dir}	48	44	61	49	55	73	65	69	°
	$U_{10,\mathrm{dir}}$	79	88	87	84	82	82	81	79	°
	U_{10}	6.0	3.6	3.6	3.6	3.6	3.6	3.6	3.7	m/s
Obs	C	–	1.2	1.4	1.6	2.1	1.8	1.2	0.3	m/s
	C_{dir}	–	40	58	60	53	54	57	195	°
	U_1	4.3	3.7	3.5	3.9	2.9	2.5	4.5	4.1	m/s
	$U_{1,\mathrm{dir}}$	110	196	200	200	27	35	189	201	°
	U_{10}	5.4	4.7	4.4	4.9	3.7	3.2	5.7	5.1	m/s

For SC5, the wind direction difference between the model (U_{10}) and measured (U_1) is $\sim 120°$. If compared with the current direction, the measured wind direction at 1 m height was about 38° related to the current direction, while the model direction differs 145° related to the current direction at 10 m height (note that the Tab.2 follows the meteo-oceanographic wind and current directions conventions). As the wind at 10 m and current are moving almost in opposite directions (145°) it is expected to have a different wind direction closer to the current direction surface at 1 m as the wind must align to the current at the boundary layer ($z = 0$, Eq.4). At SC5 the measured velocity is also 56% higher than the model and for all measured conditions, the wind is on average 26% higher than the model. Numerical wave models are forced by winds, and the wind errors are generally expected to be the largest source of error (e.g. WISE Group, 2007; Rascle and Ardhuin, 2013). Given the large discrepancy between model and observations, we have thus investigated the accuracy of the wind forcing and tested a wide range of numerical model options.

Generally, the wind forcing can be the most significant source of error in the model and cause a much stronger effect on the wind sea frequencies than the hydrodynamic current modulation. If the wind forcing is biased, it could represent a significant difference between the model results and the measurements (Fig.6). To test that, it was done a sensitivity analysis using a simple bias correction. Namely, the ECMWF forcing was multiplied by a constant factor R: $\mathbf{U}_{10}^{\mathrm{ECMWF}} \times R$. For SC4 and SC5 the correction factor is calculated based on the near-surface wind measurements from OCARINA and SWIFT, extrapolated to 10 m height (Fig. 2).

For SC1, SC2 and SC3 we do not have the local wind information, so it was corrected by an a priori constant coefficient. These numerical tests follow ST4 parameterization with the only modification in the forcing fields (see WNDxR in Tab.1). The $\mathbf{R}$ coefficient used in each SCs is explicit in legend. The results are presented in Figure 7.

The general wave energy observed at frequencies related to the wind sea spectrum was consistent with ad hoc wind corrections applied to U_{10}. For SC4 the wind bias correction was not able to give the main features of the measured wave spectra. In this case, the ship-mounted stereo video and OCARINA were both collecting data, on the edge of the structure of the current field associated with Passage du Fromveur channel, at the same time (Fig.3.d). Because the SC1, SC2, and SC3 we do not have any wind measurements the only option was to impose a local ad-hoc wind correction on the data. These results are not realistic but exemplify the scale of that wind bias impact in the numerical model.

To further explore this problem, we performed several numerical simulations considering wind forcing and other source terms. Figure 8 present the numerical test results according Tab.1.

Figure 8 show that AROME winds are more accurate for SC1, but give worse results in SC2 and SC3. In general, the AROME wind speed was lower than that given by ECMWF, further reducing the short wave energy level.

Another important aspect of wave generation by the wind is that it is the relative wind $\mathbf{U}_{10} - \mathbf{C}$ which drives the waves. In WW3, this correction on the wind speed that forces the wave growth is taken as a correction factor, with $\mathbf{U}_{\mathrm{model}} = \mathbf{U}_{10} - r_{\mathrm{wnd}}\mathbf{C}$. This effect was also found to be potentially important for tidal currents at coastal scales (Ardhuin et al, 2012). In our numerical tests, removing this relative wind effect, by taking $r_{\mathrm{wnd}} = 0$, increased the error by 1 to 20% depending on the case and frequency. SC2 is an exception with better results obtained with the default value of $r_{\mathrm{wnd}} = 1$. So the wind stress is estimated from the wind speed at 10 m after the RWND correction, where the transfer of bulk momentum is used based on MOST theory to compute the wind input in the source function. The stress direction in MOST theory is typically assumed to be in the same direction as the wind U_{10}, although measurements have shown that this is generally incorrect, with differences that can exceed 30 degrees (e.g., Drennan and Shay, 2006; Potter et al, 2015).

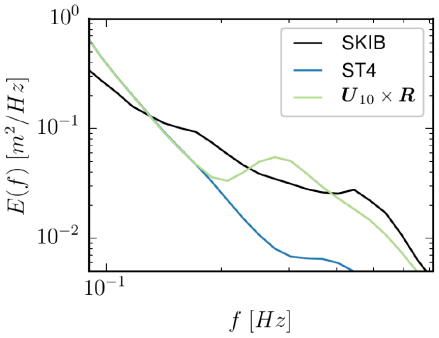

(a) SC1: from 2015/10/23 08:30 to 09:00

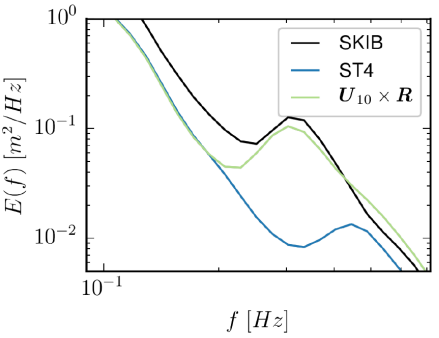

(b) SC2: from 2015/10/23 11:30 to 11:30

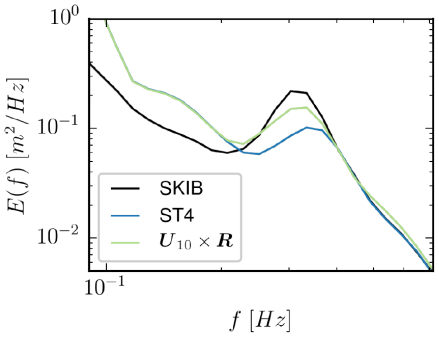

(c) SC3: from 2015/10/23 13:40 to 14:40

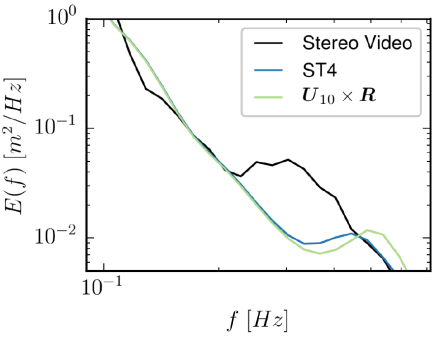

(d) SC4: from 2015/10/23 10:04 to 10:34

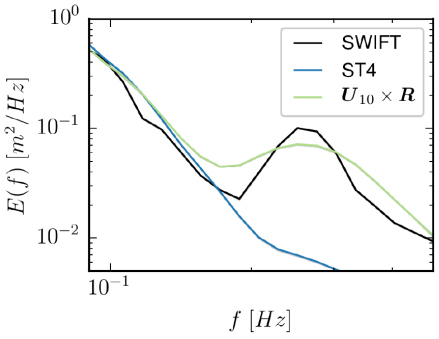

(e) SC5: from 2016/09/21 15:08 to 16:32

Fig. 7 Observation and wind sensitivity tests. The solid line represents a space and time average of the spectral density of the variance. The observation is shown in black, the blue line uses the ECMWF wind forcing and the green line is a numerical test using the $\mathbf{U}_{10}^{\mathrm{ECMWF}} \times R$ correction. For a) SC1 WNDx1.5; b) SC2 WNDx1.5; c) SC3 WNDx1.1; SC4 the WNDxR was $U \times \mathbf{-1.547}$ and $V \times \mathbf{0.878}$. For b) SC5 the WNDxR used was $U \times \mathbf{-5.864}$ and $V \times \mathbf{-0.156}$.

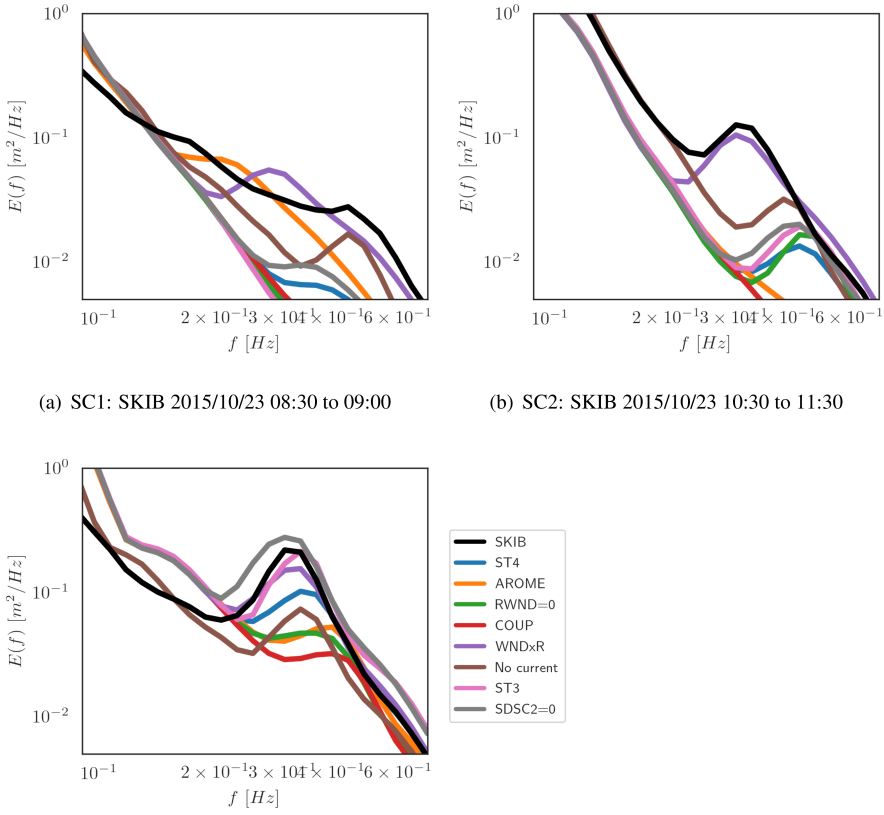

(a) SC1: SKIB 2015/10/23 08:30 to 09:00

(b) SC2: SKIB 2015/10/23 10:30 to 11:30

(c) SC3: SKIB 2015/10/23 13:40 to 14:40

Fig. 8 Observation and numerical tests. The solid line represents a space and time average of the spectral density of the variance. The observation is shown in black, the colored line follows the numerical tests presented in Table 1. WND×R is the same results presented in Fig.7, and are displayed for a comparison reference.

We also tested used the results from a coupled numerical simulation using Meso-NH and MARS3D. In the coupled ocean-atmosphere numerical experiment, the wind field was increased by about 20 to 30% in the current region. However this difference is still much lower than the one expected from the observations data acquired during the BBWAVES 2015 campaign. This coupled simulation also considered wind speed at 10 m as input and MOST theory to estimate the wind stress inside the model.

In conclusion, all the alternative wind forcing (except the theoretical WND×R) tested here were weaker than the observed wind and proof to be inefficient to reproduce the observed wind sea peak energy. After forcing, the main source of error in wave models generally comes from parameterizations (Roland and Ardhuin, 2014). To further evaluate the scenario we performed a sensitivity analysis on the current effect (running the model with or without

current, "ST4" and "No current"), in the dissipation source term (running the model with or without dissipation, "ST4" and "SDSC2=0") and concluding with an alternative input and dissipation source package ("ST3").

Running the model without current showed a significant impact at short-scale energy. In SC3, with waves and current in opposing directions (Fig.8.c) the wave energy is lower without current. The opposite is observed for SC1 and SC2, when the waves follow the current.

The ST3 parameterization from Bidlot et al (2005), is a modification of the so-called WAM Cycle4 parameterization (Janssen, 1994). When comparing model results in simulations with ST3 and ST4, SC3 is the most interesting case with realistic energy levels at high frequencies considering ST4, but with a strong underestimation at the wind sea peak. This difference is similar to the one reported by Ardhuin et al (2007), with the presence of low-frequency waves leading to a reduced value of the mean wavenumber and an artificial reduction in the short wave dissipation in ST3. At SC1 and SC2, the model generally has a wind sea peak ($f \simeq 0.25$ Hz) at a too high frequency. In these two cases, the difference between ST3 and ST4 is relatively minor. In fact, by setting the breaking dissipation to zero in ST4 ($C_{\mathrm{ds}}^{\mathrm{sat}} = 0$ in WW3, numerical test SDSC2=0 at Fig.8) hardly reduced the negative bias, so that's more than a dissipation problem it must be a problem of too low energy input, probably from the wind, possibly from the currents or the combination of wind and current.

In summary, in conditions of waves propagating in areas of strong current, several processes may have a strong impact on the energy levels of the wind sea peak. In particular, the wave generated by the wind in conditions where waves follow the current is very sensitive to wind speed errors. This is because the relative wind speed is further reduced when the current speed is subtracted so that the errors on the wind speed are relatively more important for the relative wind.

4 Discussion

In the conditions analyzed here, the errors due to parameterizations of the dissipation or non-linear source term may be important, but the major differences on short wave energies are expected to come from the wind forcing. Both numerical tests with more refined wind forcing conditions at U_{10} ("AROME" and "COUP") were weaker than ECMWF winds, resulting in a lower wind sea energy peak. However, the coupled simulation allows having more precise surface atmospheric fields (τ_s, z_0 and others) modulated by the surface current. So, a closer look at the atmospheric boundary conditions from the coupling simulation it was observed a large difference in the coupled and not coupled numerical simulations.

Figure 9 shows an example of how surface current (from MARS3D) can modify Meso-NH results. The simulation output was taken on October 23, 2015, 10:00 UTC (time corresponding to SC4). The Meso-NH results for this

time are presented on Figure 9.a, b, c and d Figure 9.a and b shows the Meso-NH wind speed at the lowest model level near to 10 m height (U_{10}) and air-sea moment flux at the ocean (τ_s) for STC and NC simulations (Fig.9.c and d).

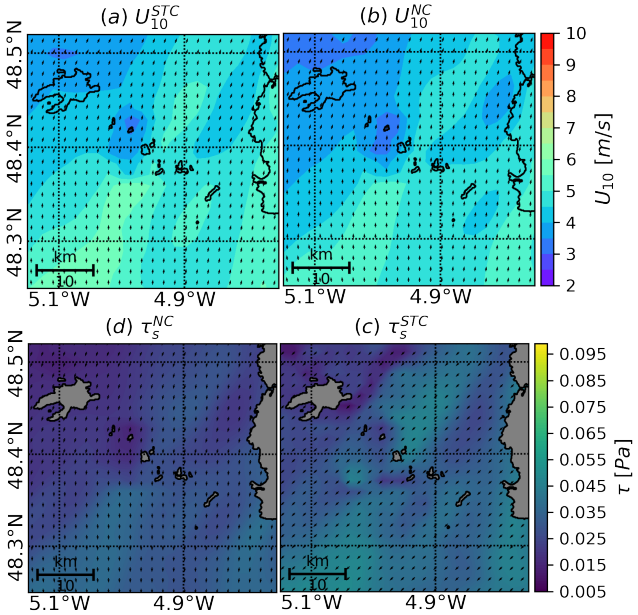

Fig. 9 Current effect on the surface wind speed. a) wind speed near a 10 m height (U_{10}) for the numerical simulation (STC) coupled with sea surface temperature and current from MARS2D; b) wind speed near a 10 m height (U_{10}) for the numerical simulation (NC) forced without current; c) Air-sea momentum flux at the ocean surface (τ_s) for STC numerical simulation, coupled with sea surface temperature and current from MARS2D; d) Air-sea momentum flux at the ocean surface (τ_s) for NC numerical simulation, without current.

Figure 9.a and b picture some differences between STC and NC simulations. A first analysis allows observing that STC present higher speeds than NC, with a minor impact in the wind direction. For evaluating closer what is happening in the oceanic and atmospheric boundary layer, Figure 9.c and d is possible to compare the air-sea moment flux τ_s for STC and NC. When comparing Figure 9.c with the current field (Fig.10.d) is possible to observe a significant reduction of τ_s over the current structures. To better quantify the differences between STC and NC, Figure 10 present the evolution of the current field, flowed by the difference between STC and NC at U_{10} (center) and τ_s (right).

In the coupled ocean-atmosphere numerical experiment, when the atmosphere adjusts to the sea surface current, the wind field is increased by about 20 to 30% around the Passage du Fromveur (Fig.10). However, the tidal current impact in the near-surface circulation was much more evident in the air-sea moment flux, where the coupled simulation with sea surface current has caused a reduction in the order of 90% in τ_s.

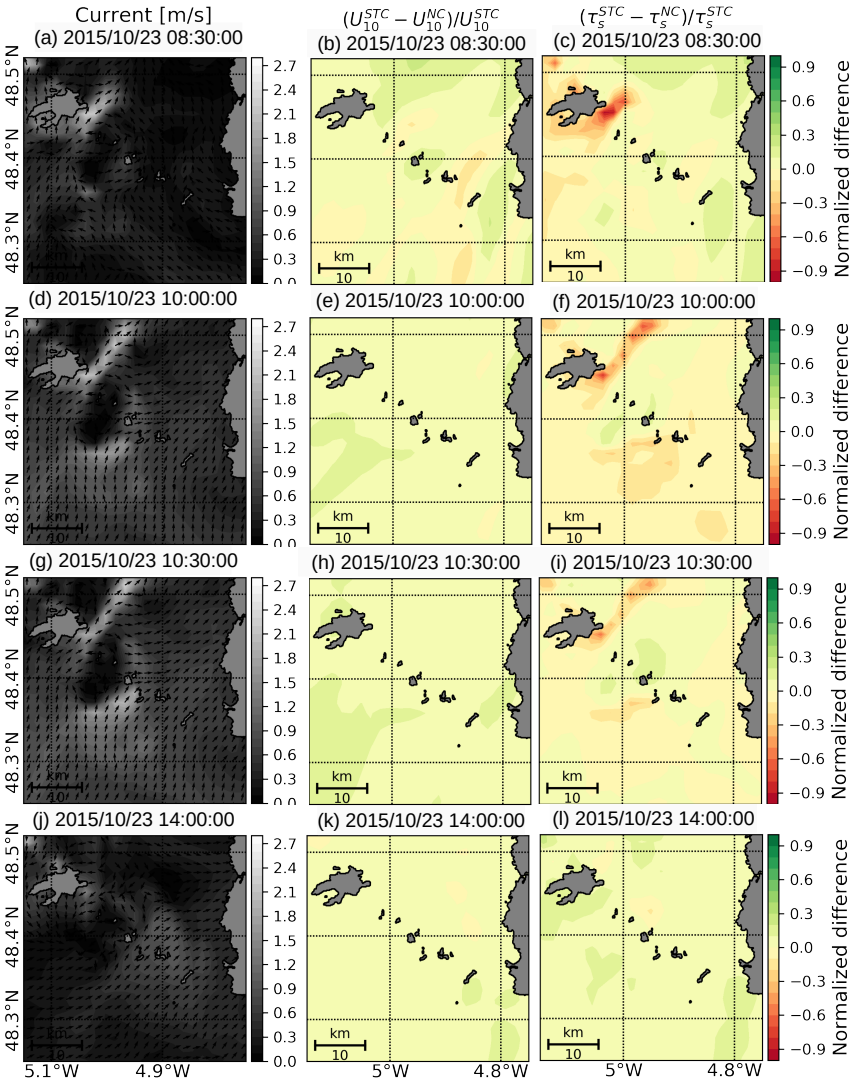

Fig. 10 Comparison between STC and NC for Meso-NH output on October 23, 2015, UTC. (a, d, g and j) shows the MARS3D current field. (a) represent the conditions observed at SC1, while (d), (g), and (j) correspond to SC4, SC2, and SC3 respectively; (b, e, h, and k) represent the normalized difference for U_{10} and (c, f, i and l) for τ_s.

By comparing the STC and NC ocean-atmosphere coupled simulations, the numerical results show that the current has a much more significant impact on the surface drag coefficient, wind shear, roughness length than at U_{10}. However, waves models usually use $\mathbf{U}_{10,\mathrm{rel}}$ (eq.4) in the routine to recomputed the friction velocity $u_\star$, considering the simplified bulk formulation (Eq.1-3), that does not require the surface–atmosphere moment fluxes are aggregated for each grid cell (for coupled or not coupled simulation). In this condition,

most of the air-sea interaction simulated at the atmospheric friction velocity is lost during this process, reducing wind-current modulation on the short wave growth. The impact of this approximation in $u_\star$ is show at Figure 11, where the results from COUP (U_{10}^{STC} and U_{10}^{NC}) were used as forcing field for WW3.

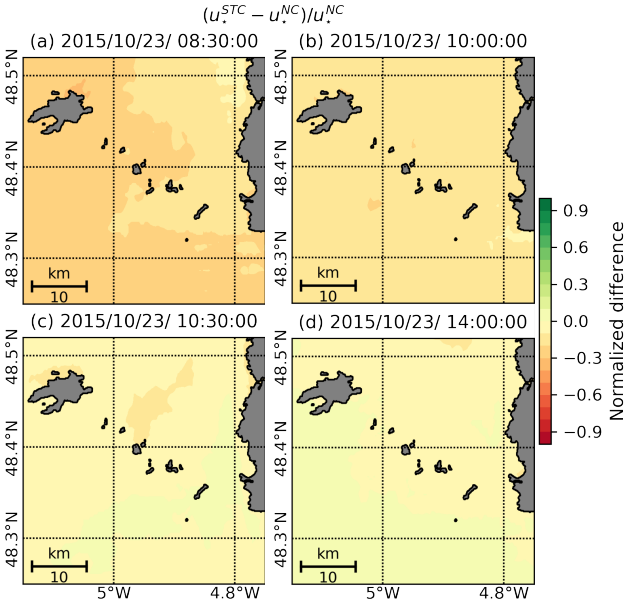

Fig. 11 Comparison between $u_\star$ at WW3, considering (COUP) U_{10}^{STC} and U_{10}^{NC} as forcing wind field. (a) represent the conditions observed at SC1, while (b), (c), and (d) correspond to SC4, SC2, and SC3 respectively. The normalized difference is computed as $(u_\star^{STC} - u_\star^{NC})/u_\star^{NC}$.

In stochastic waves models $u_\star$ is crucial to control the wind energy input and wind sea growth. From Figure 11, it is possible to observe that the current impact in $u_\star$ is practically imperceptible, especially if compared with the moment flux results at Figure 10.

The bulk formula is based on the assumption that wind does not turn between U_{10} and $u_\star$ and a perfect logarithmic wind speed decay with height. Perhaps it must be revisited for conditions dominated by currents. For example, from the near-surface measurements at SC5 (expressed in Tab.2) the winds at U_{10} were supposed to be against the current ($\sim 145°$). However, the SWIFT measurements (U_1) suggest that the winds is only 38° shifted from the current direction. Under that condition, it is expect that $u_\star$ is align with the tidal current, which is required to have a continuous momentum flux in the boundary conditions, but simply applying the bulk formula at U_{10} does not make that necessarily true.

The numerical simulations and observed results analyzed here suggest that the tidal current impact on the moment flux between the ocean and atmosphere was much more evident close to the surface than at 10 m height, and consequently, it can cause a more significant impact on $u_\star$ (τ_s, Fig.10) and on the local wind wave's growth than what was initially predicted by the wave model.

5 Conclusion

Here we used several drifting buoys in an environment with strong tidal currents to measure the wave transformations along their propagation path in various fields of coastal currents. These conditions have been difficult to reproduce numerically, presumably due to not predicted bias in the wind forcing fields leading to significant underestimation of the wind sea energy. These underestimations were systematic for all the sensors deployed and for both BBWAVES experiments, in 2015 and 2016.

By performing several numerical tests with different forcing fields and source terms parameterizations we conclude that the main source of error was in the wind forcing. This bias could not be explained by the relative wind and current correction neither by different model parameterizations, accounting for dissipation and wave-current interactions.

This scale of variation in the spectral density could be only by inaccurate local wind forcing. However, the direct impact of currents in U_{10} was not so clear to observe in the coupled simulation results. A direct link between wind and current was very evident through the air-sea moment flux. If compared with the simulation without current, the current has modified the air-sea moment flux on the scale of 90% around the Passage du Fromveur area and only 20 to 30% of variation on U_{10}. So, by forcing the wave model at U_{10} most of the coupled air-current moment flux information can be lost, resulting in an underestimation of the current impact on the local $u_\star$ and wind sea growth. The results suggest that the physical representations of some key processes, such as current effect into the surface atmospheric boundary layer require further investigations.

This possibility can be numerically solved by improving the parameterization of the empirical growth rate or by using a high-resolution coupled atmospheric friction velocity, which is not investigated in this work. Nevertheless, from these observations and numerical experiments arises a new focus on the interaction between fields of tidal currents and winds, probably not properly documented before. Complementary field observations and deeper investigation are thus required on this aspect.

Data availability. The datasets generated during the current study are available from the corresponding author on reasonable request.

Acknowledgments. Work described here is supported by DGA under the PROTEVS program, LabexMer via grant ANR-10-LABX-19-01, and CNES as part of the CFOSAT and SWOT preparatory program. We thank all the TOIS

group at LOPS, O. Peden, for his contributions to buoy tests and the crew of R/V Thalia for their performance during the BBWAVES-2016 experiment.

Author contributions. P.V. Guimarães, F. Ardhuin: Conceptualization, methodology, field experiment, numerical simulations, investigation, writing. Y. Perignon, A. Benetazzo: Conceptualization, methodology, field experiment, investigation, writing. M-N. Bouin: Field experiment, coupled air-sea numerical simulations and OCARINA data processing. M. Accensi: Discussion, field experimental and numerical simulations support. V. Garnier, J-L. Redelsperger: Discussion and coupled numerical simulation support. J. Thomson: Discussion and SWIFT data processing.

Conflict of interest. The authors declare no competing interests.

References

Ardhuin F, Herbers THC, Watts KP, et al (2007) Swell and slanting-fetch effects on wind wave growth. Journal of Physical Oceanography 37(4):908–931. https://doi.org/10.1175/JPO3039.1

Ardhuin F, Marié L, Rascle N, et al (2009) Observation and estimation of lagrangian, stokes, and eulerian currents induced by wind and waves at the sea surface. Journal of Physical Oceanography 39(11):2820–2838. https://doi.org/10.1175/2009JPO4169.1, https://arxiv.org/abs/0810.3537

Ardhuin F, Rogers E, Babanin AV, et al (2010) Semiempirical dissipation source functions for ocean waves. Part I: definition, calibration, and validation. Journal of Physical Oceanography 40(9):1917–1941. https://doi.org/10.1175/2010JPO4324.1, https://arxiv.org/abs/0907.4240

Ardhuin F, Roland A, Dumas F, et al (2012) Numerical wave modelling in conditions with strong currents: dissipation, refraction and relative wind. Journal of Physical Oceanography 42(1):2101–2118. https://doi.org/10.1175/JPO-D-11-0220.1

Benetazzo A (2006) Measurements of short water waves using stereo matched image sequences. Coastal Engineering 53(12):1013–1032. https://doi.org/10.1016/j.coastaleng.2006.06.012

Benetazzo A, Barbariol F, Bergamasco F, et al (2016) Stereo wave imaging from moving vessels: Practical use and applications. Coastal Engineering 109:114–127. https://doi.org/10.1016/j.coastaleng.2015.12.008

Bidlot J, Janssen P, Abdalla S (2005) Memorandum research department, A revised formulation for ocean wave dissipation in CY29R1. Tech. Rep. 1

Black PG, D'asaro E, Drennan WM, et al (2007) Air–sea exchange in hurricanes synthesis of observations from the coupled boundary layer

air–sea transfer experiment. Bulletin of the American Meteorological Society 88(March):357–374. https://doi.org/10.1175/BAMS-88-3-357

Bourras D, Branger H, Reverdin G, et al (2014) A new platform for the determination of air–sea fluxes (OCARINA): overview and first Results. Journal of Atmospheric and Oceanic Technology 31(1):1043–1062. https://doi.org/10.1175/JTECH-D-13-00055.1

Charnock H (1955) Wind stress on a water surface. Quarterly Journal of the Royal Meteorological Society 81(350):639–640. https://doi.org/10.1002/qj.49708135027

Chawla A, Kirby JT (2002) Monochromatic and random wave breaking at blocking points 107(C7):3067

Dodet G, Bertin X, Bruneau N, et al (2013) Wave-current interactions in a wave-dominated tidal inlet. Journal of Geophysical Research: Oceans 118(3):1587–1605. https://doi.org/10.1002/jgrc.20146, URL http://dx.doi.org/10.1002/jgrc.20146

Drennan WM, Shay LK (2006) On the variability of the fluxes of momentum and sensible heat. Boundary-Layer Meteorology 119(1):81–107. https://doi.org/10.1007/s10546-005-9010-z

Ducrocq V, Bouttier F, Malardel S, et al (2005) The Arome project, Mediterranean floods: scientific and technical answers from the (French) state. La Houille Blanche 2:39—-44

Edson J, Crawford T, Crescenti J, et al (2007) The coupled boundary layers and air-sea transfer experiment in low winds. Bulletin of the American Meteorological Society 88(March):341–356. https://doi.org/10.1175/BAMS-88-3-341

Edson JB, Jampana V, Weller RA, et al (2013) On the exchange of momentum over the open ocean 43:1589–1610. https://doi.org/10.1175/JPO-D-12-0173.1

Guimarães P, Ardhuin F, Sutherland P, et al (2018) A surface kinematics buoy (skib) for wave–current interaction studies. Ocean Science 14(6):1449–1460. https://doi.org/10.5194/os-14-1449-2018, URL https://os.copernicus.org/articles/14/1449/2018/

Guimarães PV (2018) Sea surface and energy dissipation. Theses, École centrale de Nantes

Gutshabash YS, Lavrenov IV (1986) Swell transformation in the cape Agulhas current 22(6):494–497

Hasselmann S, Hasselmann K, Allender JH, et al (1985) Computations and parameterizations of nonlinear energy transfer in a gravity-wave spectrum, Part II. Journal of Physical Oceanography 15:1378–1391

Hersbach H, Bidlot Jr (2008) The relevance of ocean surface current in the ECMWF analysis and forecast system. In: ECMWF Workshop on Ocean-atmosphere interactions,, pp 61–73

Janssen PAEM (1991) Quasi-linear theory of wind-wave generation applied to wave forecasting. Journal of Physical Oceanography 21(1):1631—-1642

Janssen PAEM (1994) Technical report No. 71: Results with a coupled wind wave model. Tech. rep., ECMWF

Janssen PAEM (2008) Progress in ocean wave forecasting. Journal of Computational Physics 227(1):3572–3594. https://doi.org/10.1016/j.jcp.2007.04.029

Komen GJ, Cavaleri L, Donelan M, et al (1994) Dynamics and modelling of ocean waves. Cambridge University Press

Kudryavtsev V, Grodsky VV, Dulov VA, et al (1995) Observations of wind in Golf Stream frontal zone. Journal of Geophysical Research 100(20):715—-727

Kudryavtsev V, Akimov D, Johannessen J, et al (2005) On radar imaging of current features: 1. model and comparison with observations 110:C07,016. https://doi.org/10.1029/2004JC002505

Lafore JP, Stein J, Asencio N, et al (1998) The Meso-NH atmospheric simulation system. Part I: Adiabatic formulation and control simulations. Annales Geophysicae 16(1):90–109. https://doi.org/10.1007/s005850050582

Lazure P, Dumas F (2008) An external-internal mode coupling for a 3D hydrodynamical model for applications at regional scale (MARS). Advances in Water Resources 31(2):233–250. https://doi.org/10.1016/j.advwatres.2007.06.010

Leckler F (2013) Observation et modélisation du déferlement des vagues. PhD thesis, Université de Bretagne Occidentale

Leibovich S (1983) The form and Dynamics of Langmuir Circulations. Annual Review of Fluid Mechanics 15(1):391–427. https://doi.org/10.1146/annurev.fl.15.010183.002135, https://arxiv.org/abs/arXiv:1011.1669v3

Masson D (1996) A case study of wave-current interaction in a strong tidal current. Journal of Physical Oceanography 26(1):359–372

Masson V, Le Moigne P, Martin E, et al (2013) The SURFEXv7.2 land and ocean surface platform for coupled or offline simulation of Earth surface variables and fluxes. Geoscientific Model Development 6:929–960. https://doi.org/10.5194/gmd-6-929-2013, URL https://hal.archives-ouvertes.fr/hal-00968042

Miles JW (1957) On the generation of surface waves by shear flows. Part 4. Journal of Fluid Mechanics 13(1):185–204. https://doi.org/10.1017/S0022112057000567

Muller H, Dumas F, Blanke B, et al (2007) High-resolution atmospheric forcing for regional oceanic model: The Iroise Sea. Ocean Dynamics 57(4-5):375–400. https://doi.org/10.1007/s10236-007-0115-4

Phillips OM (1984) On the response of short ocean wave components at a fixed wavenumber to ocean current variations. https://doi.org/10.1175/1520-0485(1984)014⟨1425:OTROSO⟩2.0.CO;2

Pineau-Guillou L (2013) Validation des modèles hydrodynamiques 2D des côtes de la Manche et de l'Atlantique. Tech. rep., Ifremer, Brest

Potter H, Collins COIII, Drennan WM, et al (2015) Observations of wind stress direction during typhoon Chaba (2010) 42:9898–9905. https://doi.org/10.1029/2011JC007833

Rapizo H, Waseda T, Babanin AV, et al (2016) Laboratory experiments on the effects of a variable current field on the spectral geometry of water waves. Journal of Physical Oceanography 46:2695—-2717. https://doi.org/10.1175/JPO-D-16-0011.1, URL http://journals.ametsoc.org/doi/10.1175/JPO-D-16-0011.1

Rapizo H, Babanin AV, Provis D, et al (2017) Current-induced dissipation in spectral wave models 122:2205–2225

Rascle N, Ardhuin F (2013) A global wave parameter database for geophysical applications. part 2: model validation with improved source term parameterization 70:174–188. https://doi.org/10.1016/j.ocemod.2012.12.001

Rascle N, Chapron B, Ponte A, et al (2014) Surface roughness imaging of currents shows divergence and strain in the wind direction. Journal of Physical Oceanography 44(8):140509140828,004. https://doi.org/10.1175/JPO-D-13-0278.1

Rascle N, Nouguier F, Chapron B, et al (2016) Surface roughness changes by fine scale current gradients: Properties at multiple azimuth view angles 46:3681–3694. https://doi.org/10.1175/JPO-D-15-0141.1

Rascle N, Molemaker J, Marié L, et al (2017) Intense deformation field at oceanic front inferred from directional sea surface roughness observations 48:5599–5608. https://doi.org/10.1002/2017GL073473

Roland A (2008) Spectral Wave Modelling on Unstructured Meshes. PhD thesis, Institut fur Wasserbau und Wasserwirtschaft

Roland A, Ardhuin F (2014) On the developments of spectral wave models: numerics and parameterizations for the coastal ocean 64(6):833–846

Sullivan PP, Mcwilliams JC (2010) Dynamics of winds and currents coupled to surface waves. Annual Reviews in Fluid Mechanics 42:19—-42. https://doi.org/10.1146/annurev-fluid-121108-145541

The WAVEWATCH III ® Development Group (2016) User manual and system documentation of WAVEWATCH III ® version 5.16. Tech. Note 329, NOAA/NWS/NCEP/MMAB, College Park, MD, USA, 326 pp. + Appendices

Thomson J (2012) Wave breaking dissipation observed with "SWIFT" drifters. Journal of Atmospheric and Oceanic Technology 29(12):1866–1882. https://doi.org/10.1175/JTECH-D-12-00018.1

Thorpe S (2004) Langmuir Circulation. Annual Review of Fluid Mechanics 36(1):55–79. https://doi.org/10.1146/annurev.fluid.36.052203.071431

Tolman HL, Accensi M, Alves H, et al (2014) User manual and system documentation of WAVEWATCH III. National Oceanic and Atmospheric Administration, National Weather Service Center for Environmental Prediction 1:311

van der Westhuysen AJ, van Dongeren AR, Groeneweg J, et al (2012) Improvements in spectral wave modeling in tidal inlet seas. Journal of Geophysical Research: Oceans 117(8):1–23. https://doi.org/10.1029/2011JC007837

Virtanen P, Gommers R, Oliphant TE, et al (2020) SciPy 1.0: Fundamental Algorithms for Scientific Computing in Python. Nature Methods 17:261–272. https://doi.org/10.1038/s41592-019-0686-2

Voldoire A, Decharme B, Pianezze J, et al (2017) The seamless and multi-model coupling between atmosphere, land, hydrology, ocean, waves and sea-ice models based on SURFEX surface model using OASIS3-MCT. Geoscientific Model Development Discussions (May):1–39. https://doi.org/10.5194/gmd-2017-91

White BS, Fornberg B (1998) On the chance of freak waves at sea 355:113–138

WISE Group (2007) Wave modelling - the state of the art 75:603–674. https://doi.org/10.1016/j.pocean.2007.05.005

Zippel S, Thomson J (2017) Surface wave breaking over sheared currents: Observations from the mouth of the Columbia river 122:3311–3328. https://doi.org/10.1002/2016JC012498